Wavelength Multiplexer (2023)

Gonçalo Alves Cavaco, *Instituto Superior Técnico, Universidade de Lisboa, Portugal*

***Abstract* — The Wavelength Division Multiplexing, or WDM, is a technology developed for applications in telecommunications with the purpose of combining numerous wavelengths signals into one single channel. The multiplexers can be used as passive or active components of WDM networks. These components, managed by external mechanisms, can be optical filters, lasers, or optical amplifiers. The aim of this research is the characterization of ring resonators with planar optical waveguides. The output response of these systems is analysed, for different configurations, dimensions, and materials by varying a set of parameters using the finite element method, FEM, implemented in *COMSOL*. The results of the output responses demonstrate that the change of dimensions, and core materials for the analysed configurations of the ring resonators allow the adjustments of the resonance wavelength number, and of the transmittance outside the resonance. Furthermore, the ring resonators can work as wavelength multiplexers, with the transmission of the resonance wavelengths.**

***Index Terms* — Multiplexer, ring resonator, optical waveguides finite element method, analytical method.**

I. INTRODUCTION

THE Wavelength Division Multiplexing, or WDM, technology concept goes back to the year of 1970 [1,2]. Since then, this technology has been a subject of research and development regarding telecommunications, whether in optical fibers, planar waveguides, or even free space transmission. Nowadays, WDM plays a significant role in optical communications networks around the planet, in a world with a constant need of faster transmission rates allied to increased bandwidth.

WDM allows the combination of several independent wavelength signals into a single optical channel. These concepts are the basis of the wavelength multiplexers, which are only a part of WDM links, as seen in Figure 1. These networks have also other components such as light sources composed by lasers, optical amplifiers, and receivers with optical filters, which can be passive or active devices. An active device has an external control mechanism which can be useful to monitor and assure a successful functionalization.

A wavelength multiplexer can be fabricated with planar optical waveguides or optical fibers. These multiplexers, which have couplers for distinct types of waveguides or fibers can be array waveguide grating or fiber grating multiplexers [4,5]. Despite the materials that are part of the multiplexers, there are several other characteristics, for example the dimensions and the coupling zones, which can influence the spectral response of these devices.

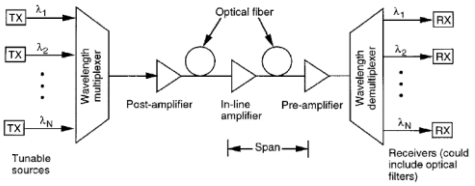

Figure 1 - Typical WDM link (from [3]).

The main goal of this research is to analyse and characterize the output response of ring resonator systems with planar optical waveguides, by doing a parameter study using the finite element method. To first characterize the ring resonator systems, it is fundamental to present the essential concepts regarding light propagation in optical waveguides and their fundamental structures. Moreover, the analysis of the parameters that influence the output response will be decisive depending on the requirements of each application and technologies. The program used for the numerical simulations of the optical systems is *COMSOL Multiphysics v5.4*. Also, to obtain the analytical models of the ring resonators, *MATLAB R2020a* is the program used.

II. LIGHT PROPAGATION AND OPTICAL WAVEGUIDES

The wave description of light was firstly introduced in the 19th century by Maxwell's equations [6,7]. This set of equations are the basis to understand the relationship between the magnetic and electrical fields and how their interaction allows the light waves to propagate at the speed of light, c_0, in vacuum. Later, Hertz experimentally confirmed the existence of electromagnetic waves and obtained the wavelength of the radiation and the propagation velocity of this waves.

The light wave propagation can be analysed considering the Maxwell's equations in a homogeneous, isotropic and a **lossless dielectric** medium. The relation between the magnetic field, $\boldsymbol{H}$, and the electrical field, $\boldsymbol{E}$, is given by the differential equations 1 and 2 where ε_0 is the electric permittivity in vacuum and μ_0 is the magnetic permeability in vacuum and the refractive index of the medium is represented by n. At vacuum, it is considered that n is unitary.

$$\nabla \times \boldsymbol{E} = -\mu_0 \frac{\partial \boldsymbol{H}}{\partial t} \quad (1)$$

$$\nabla \times \boldsymbol{H} = \varepsilon_0 n^2 \frac{\partial \boldsymbol{E}}{\partial t} \quad (2)$$

In this case, light waves can be seen as **plane waves** [8] and the magnetic and electric fields can be represented by sinusoidal functions characterized by an amplitude and an angular frequency ω. Moreover, considering a wave propagation along the z axis, the fields are presented, being

$\bar{\boldsymbol{E}}(z)$ and $\bar{\boldsymbol{H}}(z)$ the electric and magnetic phasors or complex amplitudes, respectively:

$$\boldsymbol{E}(z,t) = Re\left\{\bar{\boldsymbol{E}}(z)\, e^{j\omega t}\right\},\ \bar{\boldsymbol{E}}(z) = E_r\, e^{-j\beta z} \tag{3a}$$

$$\boldsymbol{H}(z,t) = Re\left\{\bar{\boldsymbol{H}}(z) e^{j\omega t}\right\},\ \bar{\boldsymbol{H}}(z) = H_r\, e^{-j\beta z} \tag{3b}$$

Taking into account the phasors representation of the fields with a propagation constant β and a complex amplitude accordingly to the position r in the normal plane of the z axis, it is fundamental to define the boundary conditions when the refractive index n changes, that is, when the medium changes. For lossless mediums, the tangential components of each field must be equal at the boundaries.

Moreover, light propagation happens not only in vacuum or free-space regions but also light can be confined in structures known as optical fibers or waveguides.

The two-dimensional, 2D, structure of an optical waveguide presents a core inside a cladding and/or a substrate [9]. These 2 sections of the waveguide have 2 different refractive indexes, allowing the light to be reflected at the core, that has a higher refractive index, n_{core} (n_1), when compared to the cladding's refractive index, n_{clad} (n_0). The total reflection of the light only happens if the incident angle of the light wave, θ, represented in the Figure 2, is lower than the maximum light acceptance angle, θ_{max}.

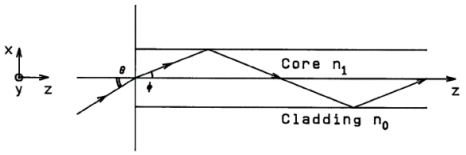

Figure 2 – Basic structure of a two-dimensional optical waveguide (from [6]).

The θ_{max} and the maximum inclination angle within the core, ϕ_{max}, can be obtained with the calculus of the relative refractive index, Δ, taking into account the equations 4, 5 and 6.

$$\Delta = \frac{n_{core}^2 - n_{clad}^2}{2n_{core}^2} \tag{4}$$

$$\theta_{max} = n_{core}\sqrt{2\Delta} \tag{5}$$

$$\sin\theta_{max} = n_{core}\ \sin\phi_{max} \tag{6}$$

Even if the incident angle of the light, θ, is smaller than the θ_{max}, light waves will only propagate inside the waveguide with a certain discrete inclination angle ϕ, dependent on the waveguide structure such as the core radius, the core refractive index, n_{core}, and the relative refractive index, Δ. This inclination angle, ϕ, also depends on the wavelength of the light, λ_0, defined as the ratio between c_0 and the frequency f. For each ϕ there is a distinct optical field called the mode. The fundamental mode is given by the minimum inclination angle.

The propagation constant β of the light wave is defined by the equation 7, as,

$$\beta = k\, n_{core} \cos\phi = k\, n_{eff} \tag{7}$$

The wavenumber of the light is represented by k, as the ratio between 2π and the vacuum wavelength λ_0. As a replacement for ϕ, the constant β can be also obtained by the effective refractive index, n_{eff}.

Furthermore, two-dimensional slab waveguides are characterized by having three main parts such as the core, the cladding, and the substrate, each one with a distinct refractive index [10]. These two-dimensional slab waveguides can be symmetric if $n_{sub} = n_{clad}$ or asymmetric if $n_{sub} \neq n_{clad}$. In this specific case, the electric and magnetic fields are independent of the y-axis, as it can be observed in the Figure 2, where it is considered the plane *xz*. Therefore, in slab waveguides only exist two independent modes, which are the transversal electric, TE, mode, where there is only electric field alongside the y-axis, and the transversal magnetic, TM, mode, where there is only magnetic field alongside the y-axis.

For the theoretical analysis of three-dimensional waveguides, particularly rectangular waveguides, there are various methods proposed by multiple authors to determine the dispersion equations. Despite these methods, with the effective index method it is possible to simplify the analysis of 3D waveguide structures onto two-dimensional structures. The finite element method, FEM, is appliable for more complex 2D waveguide structures for WDM.

The implementation of basic optical couplers has the coupled mode theory as theoretical basis to investigate the interactions of two or more light waves used in real WDM.

The first coupled mode theory description is made by Pierce and Miller in 1954 [11]. In the following years, this theory was developed and applied by other authors in optical waveguides and fiber optics. The models for the coupling scenarios are characterized by having two or more dielectric waveguides. The optical couplers are also divided into codirectional and contra directional couplers, regarding the direction of the light propagation in the waveguides.

One example of a coupler device is the ring resonator [12]. Ring resonators are made of straight and curved waveguides structures. In these coupler devices, the optical phase φ is responsible for changing the optical transmittance.

III. STATE-OF-THE-ART

For WDM technologies, one type of coupler devices that can be used is the ring resonator, RR. Ring resonators are built with distinct sizes, from a few meters to micrometers, and with distinct types of materials depending on the application requirements such as the output spectrum and the finesse [13]. In this case, the micro ring resonators, MRR, are the most important for integration in larger devices, particularly for applications in optics, such as switching [14, 15, 16], or photonics, as for example in biosensors [17] and lasers [18]. These type of optical resonators can operate also as filters [19], where the input wavelength signals are distributed in straight and curved waveguides or optical fibers, [20]. Marcatili was responsible for the simulation of an integrated ring resonator for a filter in 1969 [21].

The development of optical ring resonators began with the demonstration of the first guided optical RR by Weber and Ulrich in 1971 [22]. In 1980, Haavisto and Pajer fabricated a

RR with low loss in the waveguides, which are coupled with a larger curved region, of a few cm, via the evanescent field [23]. Two years later in 1982, the first optical glass fiber RR was built by Stokes, Chodorow, and Shaw. From this decade onwards, ring resonators were made with glass as the main material and other components that allow the change of the glass refractive index. There are also several studies with another ring resonators with silica-based glasses [24] and polymers [25, 26] in the past years.

In 1997, Rafizadeh et al. fabricated a micro-RR with a lateral coupling to bus waveguides. Afterwards, it was demonstrated that this micro-RR can be used in several applications in multi-ring devices, switches and for WDM [27]. Other technologies such as micro disks resonators, tunable ring resonators with other types of couplers were also developed with varied sizes in recent years [28, 29, 30].

RR can have numerous configurations. However, it is crucial to define the 2 basic configurations to further analyse other complex ring resonator devices. These 2 configurations have one or two straight waveguides, also called port/bus waveguides, and a ring-shaped waveguide, which is **evanescently coupled**. The single RR and the add-drop RR can be represented by Figures 3 and 4, respectively.

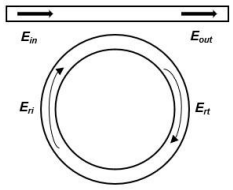

Figure 3 – Single RR.

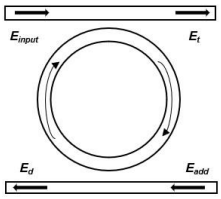

Figure 4 – Add-drop RR.

To simplify the analysis of ring resonators, it is considered that the input power is equal to the output power and the light inside the waveguides are partially transmitted in the coupling region. Regarding the simplification, the scattering matrix can be used to describe the fields. Firstly, considering the single RR, the scattering matrix is defined as in equation 8, being $\overline{\boldsymbol{E}}_{\boldsymbol{out}}$ and $\overline{\boldsymbol{E}}_{\boldsymbol{in}}$ the output field and the input field of the bus waveguide, respectively. Moreover, the fields inside the ring-shaped waveguide, $\overline{\boldsymbol{E}}_{\boldsymbol{ri}}$ and $\overline{\boldsymbol{E}}_{\boldsymbol{rt}}$, can also be related taking into account the equation 9.

$$\begin{bmatrix} \overline{\boldsymbol{E}}_{\boldsymbol{out}} \\ \overline{\boldsymbol{E}}_{\boldsymbol{rt}} \end{bmatrix} = \sqrt{1-\gamma} \begin{bmatrix} A & jB \\ jB & A \end{bmatrix} \begin{bmatrix} \overline{\boldsymbol{E}}_{\boldsymbol{in}} \\ \overline{\boldsymbol{E}}_{\boldsymbol{ri}} \end{bmatrix} \tag{8}$$

$$\overline{\boldsymbol{E}}_{\boldsymbol{ri}} = \tau\, e^{-j\phi} \overline{\boldsymbol{E}}_{\boldsymbol{rt}} \tag{9}$$

The scattering matrix is symmetrical with real coupling coefficients A and B, that are related by:

$$A^2 + B^2 = 1 \tag{10}$$

The factor τ is given by $\tau = \exp(-\rho L/2)$, being ρ the amplitude attenuation coefficient, and L is the perimeter of the ring-shaped waveguide, given by $L = 2\pi r$, with a radius, r, of the exterior circumference of the ring-shaped waveguide. The phase shift is given by $\phi = \beta L + \phi_0$, where β is the propagation constant defined as specified in equation 7 and ϕ_0 is the additional phase shift. Also, the amplitude loss coefficient is represented by γ.

Considering the relationships of the electrical fields, the ratio between the output and input fields is given by:

$$\frac{\overline{\boldsymbol{E}}_{\boldsymbol{out}}}{\overline{\boldsymbol{E}}_{\boldsymbol{in}}} = \sqrt{1-\gamma}\, \left[\frac{A - \sqrt{1-\gamma}\,\tau\, e^{-j\phi}}{1 - A\sqrt{1-\gamma}\;\tau\, e^{-j\phi}}\right] \tag{11}$$

The amplitude transmittance defined by the equation 11 is the basis to obtain the intensity transmittance factor T, which allows to characterize the transmission of the RR as function of the phase shift ϕ. The transmittance factor T is expressed below, in which the parameter x is given by $x = \sqrt{1-\gamma}\,\tau$.

$$T(\phi) = \left|\frac{\overline{\boldsymbol{E}}_{\boldsymbol{out}}}{\overline{\boldsymbol{E}}_{\boldsymbol{in}}}\right|^2 = (1-\gamma)\left[\frac{A^2 + x^2 - 2Ax\cos\phi}{1 + A^2x^2 - 2Ax\cos\phi}\right] \tag{12}$$

The minimum transmittance is obtained at resonance, defined when $\varphi = 2\pi m$, where m is an integer. Moreover, the transmittance at resonance becomes zero when $A = x$, that is, the coupling losses matches the internal losses. In this case, there is no transmission, and the RR is critically coupled.

Regarding the add-drop RR configuration, there are 4 ports, known as the input port, throughput port, drop port and add port. Considering the coupling and loss coefficients of the second bus waveguide as A_2, B_2 and γ_2, the throughput port field, $\overline{\boldsymbol{E}}_{\boldsymbol{t}}$, is given below, being $\overline{\boldsymbol{E}}_{\boldsymbol{input}}$ and $\overline{\boldsymbol{E}}_{\boldsymbol{add}}$ the input port field and the add port field, respectively. The drop port field, $\overline{\boldsymbol{E}}_{\boldsymbol{d}}$, is also given with the exchange of the fields.

$$\overline{\boldsymbol{E}}_{\boldsymbol{t}} = \sqrt{1-\gamma}\left[\frac{A - A_2\sqrt{1-\gamma_2}\,x\,e^{-j\phi}}{1 - A_2\sqrt{1-\gamma_2}\,A\,x\,e^{-j\phi}}\right]\overline{\boldsymbol{E}}_{\boldsymbol{input}} - \frac{BB_2\sqrt{1-\gamma}\sqrt{1-\gamma_2}\,\sqrt{\tau}\,e^{-j\phi/2}}{1 - A_2\sqrt{1-\gamma_2}\,A\,x\,e^{-j\phi}}\,\overline{\boldsymbol{E}}_{\boldsymbol{add}} \tag{13}$$

$$\overline{\boldsymbol{E}}_{\boldsymbol{d}} = \sqrt{1-\gamma}\left[\frac{A - A_2\sqrt{1-\gamma_2}\,x\,e^{-j\phi}}{1 - A_2\sqrt{1-\gamma_2}\,A\,x\,e^{-j\phi}}\right]\overline{\boldsymbol{E}}_{\boldsymbol{add}} - \frac{BB_2\sqrt{1-\gamma}\sqrt{1-\gamma_2}\,\sqrt{\tau}\,e^{-j\phi/2}}{1 - A_2\sqrt{1-\gamma_2}\,A\,x\,e^{-j\phi}}\,\overline{\boldsymbol{E}}_{\boldsymbol{input}} \tag{14}$$

The transmittance factors of the add-drop RR configuration, taking into account only the input port, for the throughput port and the drop port are given below, in which the parameter x_2 is given by $x_2 = \sqrt{1-\gamma_2}$.

$$T_{through}(\phi) = \left|\frac{\overline{\boldsymbol{E}}_{\boldsymbol{t}}}{\overline{\boldsymbol{E}}_{\boldsymbol{input}}}\right|^2 = (1-\gamma)\left[\frac{A^2 + A_2^2x_2^2x^2 - 2AA_2x_2x\cos\phi}{1 + A_2^2A^2x^2x_2^2 - 2AA_2x_2x\cos\phi}\right] \tag{15}$$

$$T_{drop}(\phi) = \left|\frac{\overline{\boldsymbol{E}}_{\boldsymbol{d}}}{\overline{\boldsymbol{E}}_{\boldsymbol{input}}}\right|^2 = (1-\gamma)\left[\frac{(1-A^2)(1-A_2{}^2)\,x_2^2\tau}{1 + A_2^2A^2x^2x_2^2 - 2AA_2x_2x\cos\phi}\right] \tag{16}$$

On resonance, and taking into account only the input port, the transmittance of the throughput port becomes zero if the add-drop ring resonator is lossless, in which $\rho = \gamma = \gamma_2 = 0$, and if the couplers coefficients are equal.

Beyond the determination of the transmittance factors, as the fundamental output response as function of the wavelength λ, the radius r and the effective index; RRs can be analysed and characterized by other important 4 figures of merit, like the free spectral range, FSR, the resonance width or full width at half maximum, FWHM, the finesse, and the quality factor.

The FSR is defined as the difference between two consecutive resonance wavelengths. This figure of merit is

given in equation 18, being the derivative of the constant β considering the resonance wavelength, λ_{res}, as expressed in equation 17. The group refractive index is represented by n_g.

$$\frac{\partial\beta}{\partial\lambda} = -\frac{k}{\lambda_{res}}\left(n_{eff} - \lambda_{res}\frac{\partial n_{eff}}{\partial\lambda}\right) = -\frac{\beta}{\lambda_{res}} + k\frac{\partial n_{eff}}{\partial\lambda} \quad (17)$$

$$\text{FSR} = -\frac{2\pi}{L}\left(\frac{\partial\beta}{\partial\lambda}\right)^{-1} = \frac{\lambda_{res}^2}{n_g L} \quad (18)$$

The FWHM can be defined as δλ in terms of the wavelength. This parameter depends on the configuration used for the ring resonator. The expression of the FWHM for the add-drop RR is given in equation 19.

$$\text{FWHM} = \delta\lambda = \frac{\lambda_{res}^2}{\pi L n_{eff}}\frac{(1-xx_2AA_2)}{\sqrt{xx_2AA_2}} \quad (19)$$

The finesse, F, can be obtained from the ratio between the FSR and the FWHM, and the quality factor, Q, can be expressed as function of the finesse, defined in equation 20, as given in equation 21.

$$F = \frac{\text{FSR}}{\text{FWHM}} \quad (20)$$

$$Q = \frac{\lambda_{res}}{\text{FWHM}} = \frac{\lambda_{res}}{\text{FSR}}F = \frac{n_g L}{\lambda_{res}}F \quad (21)$$

In addition to considering these parameters above and the theoretical description of the ring resonators, it is fundamental to describe the finite element method and the program behind the simulations of the ring resonators.

IV. Finite Element Method and *COMSOL*

The concept of FEM has been present since 1960, when it was first used by Clough [31,32] in his paper. Although, this method started to be developed by Courant [33] and Hrenikoff [34] over structural projects. Initially, the FEM was applied for solid and fluid mechanics in a steady-state analysis before the widespread use in a variety of engineering problems, reported by Zienkiewicz and Cheung in 1965 [35]. Nowadays it is possible to find numerous software programs based on the FEM and capable of design all sort of complex geometries, for a wider range of applications and engineering fields, like electromagnetism and acoustics, to analyse time-independent and propagation problems.

The FEM is a numerical method in which the partial difference equations, PDE, that rule a complex system are approximated by the junction of elements defined by simpler equations. These elements are obtained by space discretization of the system, considering its initial and boundary conditions represented in nodal points, where the field variables of the system are known. The choice of the number and geometry of the elements, and the simpler equations may depend on the desired minimum error and/or other associated criteria.

Moreover, the FEM can be applied on a system by doing a FEA, characterized by 3 steps [36].

The first step, known as pre-processing, consists of designing the complex geometry of the system, defining the material properties, the boundary conditions, given the field variables, and discretizing the system by creating a mesh. The second step, known as processing, consists of establishing the procedure to determine the equations for each element of the system and then solving the equations for the entire system, obtaining the field variables defined at the nodal points. The last step, known as post-processing, consists of analysing the results, such as the field variables, surface and 2D plots, and testing the model for different parameters, by changing the material properties and the boundary conditions.

Considering the FEA and the advantages of the FEM for application in complex systems, this method is used to characterize and analyse WDM optical systems, using the *COMSOL Multiphysics* software. Additionally, it is essential to introduce the main configurations of the *COMSOL Multiphysics* used for the simulated RR models.

To describe and examine an RR model, firstly, the global parameters are defined in the model builder. Then, a component is created with the definitions including the boundary system and the global variable probes, which are the variables required to do the analysis of the optical systems afterwards. The geometry of the optical system is also established, and the physics are determined by the wave optics module, designed to help solving electromagnetic wave problems regarding optical applications.

The physics interface chosen is The Electromagnetic Waves, Frequency Domain Interface (*ewfd*). This interface is needed for systems with plane waves, in which the fields are seen as phasors. Furthermore, the electric field is determined as a three-component vector with a formulation of a full field as default. Moreover, in this interface, 9 nodes are added for the description of the equations and boundaries. The first node is the Wave Equation, Electric 1, where is it defined the equation and the electric displacement field model. The equation for this node is presented below in equation 22.

$$\nabla \times (\nabla \times \boldsymbol{E}) - k^2 n^2 \boldsymbol{E} = 0 \quad (22)$$

The refractive index is the electric displacement field selected, being user defined for the real part as the core refractive index, n_{core}, and for the imaginary part as zero, being both isotropic. The second node is the Wave Equation, Electric 2, stated with the same equation and the same electric displacement field employed apart from using the real part of the substrate refractive index, n_{sub}. The initial null values of the electric field components are indicated in the third node known as Initial Values. The other 6 nodes are relative to the boundaries and ports of the system, defined as perfect electric conductors. The Port 1 is the only input port of the system and there is a scattering boundary condition.

After the creation of the component branch of the model builder, the formed study is determined by a parametric sweep of wavelengths. The mesh is a physics-controlled mesh with a maximum element size governed by the study.

The final branch of the model builder is known as the results, which includes the data sets of the solutions, the tables, and the plots of the global variables, defined in the component branch. As part of the physics interface, it is also possible to obtain the electric field profile and the output

transmittances of the optical systems. These transmittances are equal to the square modulus of the scattering parameters.

Moreover, the *COMSOL* library of materials is available.

V. Add-drop RR: Description and Analysis

The add-drop RR is the first optical system characterized taking into account the FEA. In this initial step, the ring-shaped waveguide is represented with a circle and an inner layer at the centre of the substrate which is defined as a square. The 2 straight waveguides are represented as rectangles with the same height as the substrate and the same width defined as *w*.

Besides the geometrical model of the add-drop RR, the domains of the system are defined for the processing. For the add-drop RR, there are 3 domains with different fundamental equations; the core domain with a real refractive index n_{core}, the substrate domain with a real refractive index n_{sub}, and the boundary domain defined as a perfect electric conductor which has no internal electric field. The 4 ports are represented in the boundary domain being the Port 1 the input port where occurs the wave excitation. Considering the domains for the system, the mesh is created with extremely fine triangular elements.

For the numerical simulation, the dimensions of the ring resonator are defined by a radius, *r*, of the ring-shaped waveguide, with 2,5 μm, a distance, *d*, between waveguides of 0,232 μm and a thickness, *w*, of 0,3 μm for each waveguide. The refractive indexes of the waveguides, n_{core} and n_{sub}, are equal to 3,2 and 1, respectively. The reference wavelength, λ_0, is equal to 1 μm, being f_0, the reference frequency. Besides, the add-drop RR can be represented by the Figure 5, with a substrate square area of 196 μm^2.

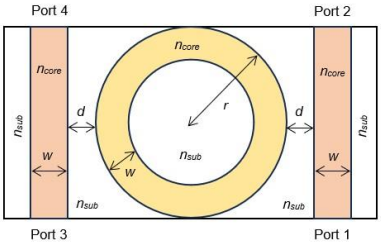

Figure 5 – The 2D representation of the add-drop RR for the numerical simulation.

After making the representation of the add-drop RR, the wave and boundary equations, the initial values for the fields, and the 4 ports are defined, being the port 1 the input port with an injected power of 1 W (reference power). To analyse and obtain the transmittances of the RR, a parametric sweep, a boundary mode analysis for each port and a frequency domain study are performed for each wavelength. For the parametric sweep, the wavelength is specified from 1420 nm to 1620 nm, with an interval of 0,2 nm for each result. The boundary mode analysis is implemented considering the effective mode index for two-dimensional problem analysis. The transmittances of the output ports 2 and 3, the throughput and drop ports, respectively, of the RR are given by the Figure 6.

Taking into account the Figure 6 and the results from the numerical simulation, the transmittance of the throughput port is around 0.8 in almost all wavelengths, except for the 5 resonant peaks. Regarding the drop port, the transmittance is practically zero, except for the same resonant wavelengths. These results show that this add-drop RR is capable of filtering and splitting the signal, as expected, considering previous analysis of the RR performance based on the theoretical basis by Hiremath [37, 38].

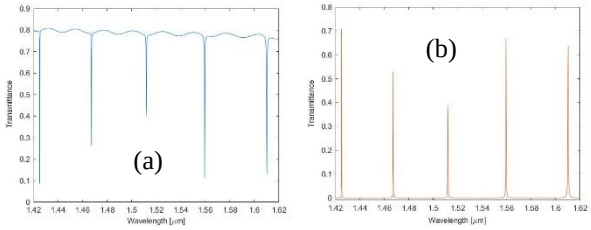

Figure 6 – Transmittances of the add-drop RR: (a) – port 2, (b) – port 3.

This representation of an add-drop RR is the basis of the analysis for ring resonators systems with numerous waveguides and different parameters, such as the radius of the ring-shaped waveguide.

Likewise, and considering the transmittance results and the theoretical equations 15 and 16 for the add-drop RR, it is possible to determine the coupling and loss coefficients and obtain the analytical model of the add-drop RR. For this model, it is considered that the intensity loss coefficients are equal for both couplers, $\gamma = \gamma_2$. As defined in the state-of-the-art, the resonance occurs when the phase shift φ is a multiple of 2π, that is, the cos φ is unitary and the transmittance is minimum for the throughput port and maximum for the drop port. When the cos φ is equal to -1, the transmittance is maximum for the throughput port and minimum for the drop port. Therefore, the maximum and minimum transmittances of the ports 2 and 3 can be defined by the equations below.

$$T_{2_{max}} = (1-\gamma)\frac{(A+A_2(1-\gamma)\tau)^2}{(1+AA_2(1-\gamma)\tau)^2} \quad (23)$$

$$T_{2_{min}} = (1-\gamma)\frac{(A-A_2(1-\gamma)\tau)^2}{(1-AA_2(1-\gamma)\tau)^2} \quad (24)$$

$$T_{3_{max}} = (1-\gamma)\frac{(1-A^2)(1-A_2{}^2)(1-\gamma)\tau}{(1-AA_2(1-\gamma)\tau)^2} \quad (25)$$

$$T_{3_{min}} = (1-\gamma)\frac{(1-A^2)(1-A_2{}^2)(1-\gamma)\tau}{(1+AA_2(1-\gamma)\tau)^2} \quad (26)$$

The values of the T_{2min} and the T_{3max} are determined by doing the mean of the transmittances obtained in resonance for each port. The T_{2max} is determined by the mean of the maximum transmittances obtained in between two resonance peaks for port 2. The T_{3min} is determined by the mean of the minimum transmittances obtained in between two resonance peaks for port 3. Considering the results obtained for this model, the mean values obtained are presented in the Table 1.

Table 1 – Mean transmittance values for the add-drop RR.

T_{2min}	T_{3max}	T_{2max}	T_{3min}
0,19997	0,58531	0,79037	9,4918 x 10^{-5}

Taking into account the mean results from the Table 1 and knowing that the coupling coefficients have a modulus less than 1 and the amplitude factor, τ, is a real positive number, there are 2 possible solutions for both coupling coefficients, being $|A| \approx 0{,}9811$ and $|A_2| \approx 0{,}9937$, and a unique solution for the losses, with $\tau \approx 1{,}265$ and $\gamma \approx 0{,}2095$, being the coupling lossless with $(1-\gamma)\,\tau \approx 1$. Besides the determination of the coupling and loss coefficients, it is also necessary to obtain the phase shift, φ, to calculate the transmittance factors of the throughput and drop ports. For this reason, the effective refractive index, n_{eff}, and the additional phase shift, φ_0 must be determined. These 2 parameters are calculated considering the resonance condition of the phase shift, being 2π the distance between 2 resonance peaks. Consequently, the effective refractive index, n_{eff}, and the additional phase shift φ_0 are determined by the equations 27 and 28, being m, the index of the resonance wavelength considered, taking into account the indexes of the Table 2.

$$n_{eff} = \frac{1}{L\left(\frac{1}{\lambda_m} - \frac{1}{\lambda_{m+1}}\right)} \tag{27}$$

$$\phi_0 = 2\pi \left(1 - \frac{n_{eff}\,L}{\lambda_m}\right) \tag{28}$$

As in this case there are more than 2 resonance peaks, the effective refractive index is a mean value considering the resonance wavelengths presented in the Table 2. The φ_0 can be obtained from any resonance wavelength. In this scenario, it is chosen the first resonance wavelength.

Table 2 – Resonance wavelengths, in μm, of the add-drop RR.

λ_1	λ_2	λ_3	λ_4	λ_5
1,4250	1,4672	1,5118	1,5594	1,6102

Considering Table 2 and the theoretical equations, 26 and 27, $n_{eff} \approx 3{,}1150$ and $\varphi_0 \approx -33{,}778 * 2\pi$.

Through the calculus of the coefficients for the application of the theoretical equations, the transmittances of the output ports for the analytical model can be represented by Figure 7.

In addition to considering the add-drop RR with a radius, r, of 2,5 μm, it is also examined 4 other models, 2 with smaller radii of 2,0 μm and 1,5 μm and 2 with different core materials. The core materials can be optically characterized by their complex refractive index, which depend on the chosen wavelength. In this models, the wavelength considered is the centre wavelength of the optical analysis, $\lambda = 1{,}52$ μm, and the imaginary part of the refractive index for both materials can be neglected. Thus, the 2 chosen materials, modelled by Marple [39,40] in 1964, are the zinc selenide, ZnSe, with a real refractive index of 2,45 and the cadmium telluride, CdTe, with a real refractive index of 2,74. All the other parameters are kept the same as much as the physical domains defined and the post-processing procedures.

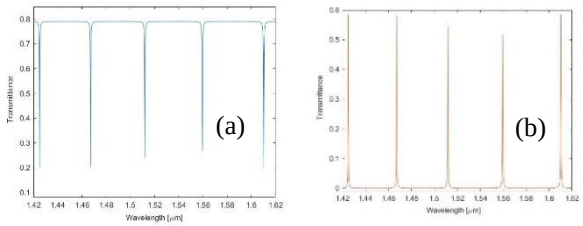

Figure 7 – Transmittances of the RR for the analytical model: (a) – port 2, (b) – port 3.

Considering the results of the simulated add-drop RR models with different radii and core materials, the transmittances of the throughput and drop ports can be presented as seen in the Figure 8.

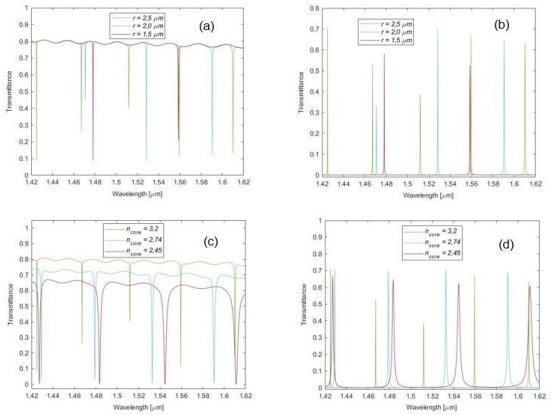

Figure 8 – Transmittances of the RR models:

(a) – port 2 and (b) – port 3 : with different radii.

(c) – port 2 and (d) – port 3 : with different n_{core}.

Taking into account the results for the distinct add-drop RR models with different parameters, the maximum transmittance is approximately equal for the add-drop RR models with different radii. However, the maximum and minimum transmittances drop with the decrease of the core refractive index. Despite the proximity between the first resonance peaks for the models with varied materials, the other resonance peaks are easier to distinguish, due to the increased FSR for higher core refractive indexes. For the models with different radii, the number of resonance wavelengths decreases with the decrease in the radius. Thus, the change of the radius permits the tuning of the number of output resonance wavelengths of the ring resonators.

Although the determination of the analytical models for the add-drop RRs, it is essential to obtain the FSR, the FWHM, the finesse and the Q factor to better characterize the RRs.

Hence and considering the equations for the 4 parameters mentioned, defined in the state-of-the-art, the results, except the Finesse, in terms of the resonance wavelengths for each model, are presented in Table 3, considering the loss coefficients equal, $\gamma = \gamma_2$, and the simplification: $n_g \approx n_{eff}$.

Table 3 – The results of the FSR, FWHM, and *Q*, for the RR with different radii and core materials.

Model	λ_m [μm]	Δλ [nm]	δλ [nm]	*Q*
RR with a *r* of **2,5 μm**	λ_1 = 1,4250	40,975	0,33221	4289,5
	λ_2 = 1,4672	43,437	0,35217	4166,1
	λ_3 = 1,5118	46,118	0,37391	4043,2
	λ_4 = 1,5594	49,068	0,39783	3919,8
	λ_5 = 1,6102	52,317	0,42417	3796,1
RR with a *r* of **2,0 μm**	λ_1 = 1,4708	55,388	0,29772	4940,2
	λ_2 = 1,5284	59,812	0,32150	4754,0
	λ_3 = 1,5906	64,779	0,34820	4568,1
RR with a *r* of **1,5 μm**	λ_1 = 1,4782	76,253	0,29570	4998,9
	λ_2 = 1,5586	84,773	0,32875	4741,0
RR with a n_{core} of **2,45**	λ_1 = 1,4272	54,329	4,0660	351,01
	λ_2 = 1,4836	58,707	4,3937	337,67
	λ_3 = 1,5446	63,634	4,7623	324,33
	λ_4 = 1,6112	69,240	5,1820	310,92
RR with a n_{core} of **2,74**	λ_1 = 1,4290	48,394	0,9088	1572,3
	λ_2 = 1,4790	51,840	0,9736	1519,2
	λ_3 = 1,5328	55,680	1,0457	1465,8
	λ_4 = 1,5906	59,958	1,1260	1412,6

The finesse, taking into account the Table 3, is, **123,34** for the initial model, **186,04** for the RR with a radius of 2,0 μm, **257,87** for the RR with a radius of 1,5 μm, **13,3618** for the RR with a n_{core} of 2,45 and **53,2476** for the RR with a n_{core} of 2,74.

In view of the results from the Table 3, as the resonance wavelength increases for each model, the FSR increases as expected considering the equation 18, defined in the state-of-the-art. As observed, with the increase of the resonance wavelength within each model, the FWHM increased and the quality factor decreased, as predicted. Nonetheless, the FWHM of each resonance wavelength for the model with the lower refractive index is around 4 or 5 times higher than the FWHMs of the model with a refractive index of 2,74. Consequently, the quality factors are up to 4 or 5 times lower for the add-drop RR model with a lower refractive index. Also, the finesse is higher for the models with a higher refractive index and a smaller radius, due to the lower FWHM and higher FSR.

The results of the add-drop RR models with different radii and core materials show that the FSR is the crucial parameter when considering the dimensions of the RR model and the FWHM is the fundamental parameter when considering the core material.

VI. Add-drop double RR: Description and Analysis

The add-drop double RR is the second optical system that is studied taking into account the analytical analysis and the FEA. This serially coupled RR model has one more ring-shaped waveguide than the previous add-drop RR model and its configuration can be represented by the Figure 9.

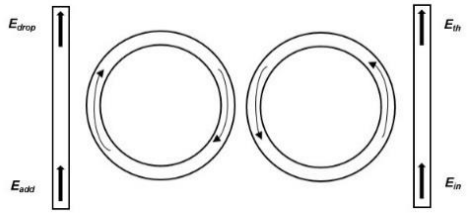

Figure 9 – Add-drop double RR.

To simplify the analytical analysis of the add-drop DRR, it is considered that the input power is equal to the output power, and the light inside the waveguides are partially transmitted in the coupling region. Regarding the simplification and for this system onwards, the signal flow graph method [41,42] along with the Mason's rule can be used to describe the relationship between the output and input fields.

Therefore, the ratio between the drop field, $\overline{\boldsymbol{E}}_{\boldsymbol{drop}}$, and the input field, $\overline{\boldsymbol{E}}_{\boldsymbol{in}}$, and the ratio between the throughput field, $\overline{\boldsymbol{E}}_{\boldsymbol{th}}$, and the input field are given by the equations 29 and 30.

$$\frac{\overline{E}_{th}}{\overline{E}_{in}} = \sqrt{1-\gamma}\left[\frac{A - A_2\,(1+AA_3)\,(1-\gamma)\tau\, e^{-j\phi} + A_3\,(1-\gamma)^2\tau^2\, e^{-j2\phi}}{1 - A_2\,(A+A_3)\,(1-\gamma)\tau\, e^{-j\phi} + AA_3\,(1-\gamma)^2\tau^2\, e^{-j2\phi}}\right] \quad (29)$$

$$\frac{\overline{E}_{drop}}{\overline{E}_{in}} = \sqrt{1-\gamma}\left[\frac{BB_2B_3(1-\gamma)\,\tau\, e^{-j\phi}}{1 - A_2\,(A+A_3)\,(1-\gamma)\tau\, e^{-j\phi} + AA_3\,(1-\gamma)^2\tau^2\, e^{-j2\phi}}\right] \quad (30)$$

For simplification of the analytical model of the add-drop DRR, it is considered that the intensity loss coefficients are equal for all the couplers, $\gamma = \gamma_2 = \gamma_3$. The real coupling coefficients are represented as A, A_2, A_3 and B, B_2 and B_3, which follow the same relation for each coupling defined by equation 10. The factor τ and the optical phase ϕ are defined in the same way as presented in the state-of-the-art.

Taking into account the equations 29 and 30, the transmittances of the throughput and drop ports are given by the equations 31 and 32, being C_1, C_2 and C_3 real coefficients defined in equation 33.

$$T_{th}(\phi) = (1-\gamma)\left[\frac{A^2 + {C_1}^2 + {C_2}^2 - 2C_1\,(A+C_2)\cos(\phi) + 2AC_2\cos(2\phi)}{1 + {C_3}^2 + A^2{C_2}^2 - 2C_3\,(1+AC_2)\cos(\phi) + 2AC_2\cos(2\phi)}\right] \quad (31)$$

$$T_{drop}(\phi) = (1-\gamma)\left[\frac{(1-A^2)(1-{A_2}^2)(1-{A_3}^2)(1-\gamma)^2\tau^2}{1 + {C_3}^2 + A^2{C_2}^2 - 2C_3\,(1+AC_2)\cos(\phi) + 2AC_2\cos(2\phi)}\right] \quad (32)$$

$$\begin{cases} C_1 = A_2\,(1+AA_3)\,(1-\gamma)\,\tau \\ C_2 = A_3\,(1-\gamma)^2\tau^2 \\ C_3 = A_2\,(A+A_3)\,(1-\gamma)\,\tau \end{cases} \quad (33)$$

Considering the results for the add-drop DRR, it is possible to determine the coupling and loss coefficients and obtain the analytical models of the add-drop DRR. To further simplify the analytical models, it is assumed that the coupling is lossless, that is, $(1 - \gamma)\ \tau = 1$, and the outer coupling coefficients are equal, $A = A_3$. As defined for the add-drop ring resonator, the maximum and minimum of the cos φ allows the determination of the expressions for the maximums

and minimums transmittances of the throughput and drop ports. Therefore, the maximum and minimum transmittances of the ports 2 and 4 can be defined by the equations below.

$$T_{2_{max}} = (1-\gamma)\frac{\left(2A+A_2(1+A^2)\right)^2}{(1+2AA_2+A^2)^2} \quad (34)$$

$$T_{2_{min}} = (1-\gamma)\frac{\left(2A-A_2(1+A^2)\right)^2}{(1-2AA_2+A^2)^2} \quad (35)$$

$$T_{4_{max}} = (1-\gamma)\frac{(1-A^2)^2\left(1-{A_2}^2\right)}{(1-2AA_2+A^2)^2} \quad (36)$$

$$T_{4_{min}} = (1-\gamma)\frac{(1-A^2)^2\left(1-{A_2}^2\right)}{(1+2AA_2+A^2)^2} \quad (37)$$

The values of the T_{2min} and the T_{4max} are determined in the same manner as for the add-drop RR. The other 2 transmittances are calculated in a similar way, considering the interval of wavelengths for the mean values defined between the centre wavelengths of each 2 resonance peaks. The method for obtaining the n_{eff} and the additional phase shift is identical as for the add-drop RR, apart from using the central wavelengths between 2 resonance peaks. Moreover, it is only used 3 of the 4 equations for the calculus of the 3 coefficients, γ, A and A_2, being the equation 35, or 36, neglected. The transmittances of the ports 2 and 4, for the simulated and analytical double RR models, are presented in Figure 10.

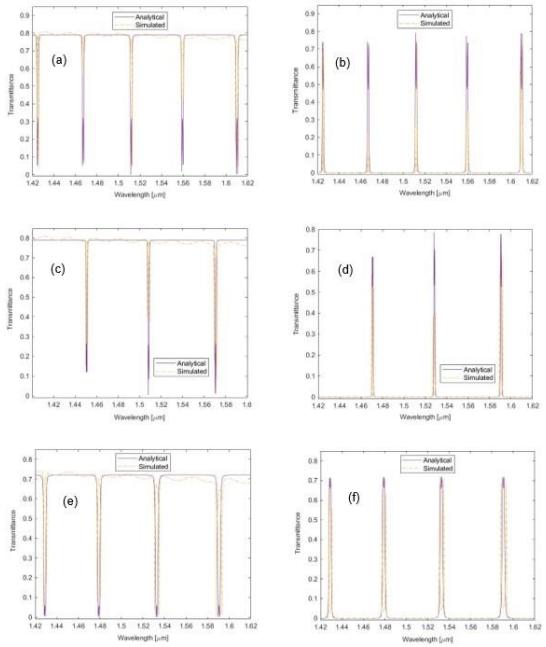

Figure 10 – Transmittances of the DRR models:

(a) – port 2 and (b) – port 4 : with a r = 2,5 μm.

(c) – port 2 and (d) – port 4 : with a radius of 2,0 μm.

(e) – port 2 and (f) – port 4 : with a n_{core} of 2,74.

Considering the results of the transmittances for each DRR model described, the main change, given the respective transmittances of the single RR models with the same parameters, is the number of resonance wavelengths, which doubles. This happens because these DRRs are over-coupled. In this scenario, resonance splitting occurs surrounding the central resonance wavelengths of the single RRs. This phenomenon is dependent on the coupling coefficients A and A_2, and it takes place when A_2 is lower than the critical coupling factor. The definition of the critical coupling factor is obtained in view of the equation 35 and the lossless coupling, being defined by the equation 38, for null transmittance.

$$A_{2_{crit}} = \frac{2A}{1+A^2} \quad (38)$$

For the critical coupling state, the FSR would be the same in each central resonance wavelength. Nevertheless, the FWHM, for each central resonance wavelength, would be distinct due to his dependence on the configuration of the RR. Hence, the quality factor and the finesse would also change.

The analytical resonance wavelengths are slightly different from the simulated ones. This variation occurs because of the simplifications assumed for the analytical DRR models. The change of the transmittance values in resonance between the results from the analytical and simulated models are due to the mean values assumed for the calculus of the coefficients and the approximate solutions obtained.

VII. Add-drop triple RR: Description and Analysis

The add-drop triple RR is the third and last optical system that is studied taking into account the analytical analysis and the FEA. This serially coupled RR model has two more ring-shaped waveguides than the first add-drop RR model and its configuration can be represented by the Figure 11.

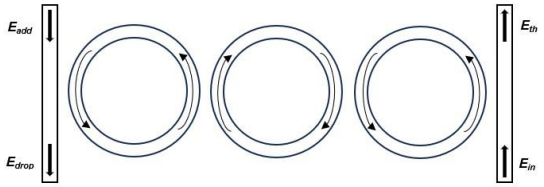

Figure 11 – Add-drop triple RR.

The analytical analysis of the add-drop TRR is done considering that the input power is equal to the output power, and the light inside the waveguides are partially transmitted in the coupling region. Regarding this simplification and taking into account the method used for the add-drop double RR to describe the relationship between the output and input fields, the ratio between the drop field and the input field and the ratio between the throughput field and the input field for the TRR model, are obtained.

For the add-drop TRR analytical model, it is considered that the amplitude loss coefficients are equal for all couplers. The real coupling coefficients are represented as A, A_2, A_3, A_4 and B, B_2, B_3 and B_4, which follow the same relation for each coupling defined by equation 10. The transmission factor τ and the optical phase ϕ are defined in the same way as presented for the other ring resonators.

Given the transmittance results and the theoretical equations for the add-drop TRR, it is possible to determine the

coupling and loss coefficients and obtain the analytical model of the TRR. To further simplify the analytical model, it is assumed that *(*1 - *γ) τ* = 1, accordingly to lossless coupling. Likewise, the outer and internal coupling coefficients are equal, A = A_2 = A_3 = A_4. As defined for the other ring resonators, the maximum and minimum of the cos ϕ allow the determination of the expressions for the maximums and minimums transmittances of the throughput and drop ports. Therefore, the minimum transmittance of the port 3 and the maximum transmittance of the port 2 can be defined by the equations 39 and 40, being T_{2min} equal to zero and T_{3max} equal to one, with these simplifications.

$$T_{2_{max}} = (1-\gamma)\frac{16\,(A+A^3)^2}{(1+A^4+6A^2)^2} \quad (39)$$

$$T_{3_{min}} = (1-\gamma)\frac{(1-A^2)^4}{(1+A^4+6A^2)^2} \quad (40)$$

These 2 mean transmittances values are calculated in a similar way as before for the other RR models, considering the interval of wavelengths for the mean values defined between the central wavelengths of each 3 resonance peaks. The method for obtaining the effective refractive index, n_{eff}, and the additional phase shift is identical, apart from using the central wavelengths of each 3 resonance peaks. The transmittances of the ports 2 and 3, for the simulated and analytical triple RR models, are presented in Figure 12.

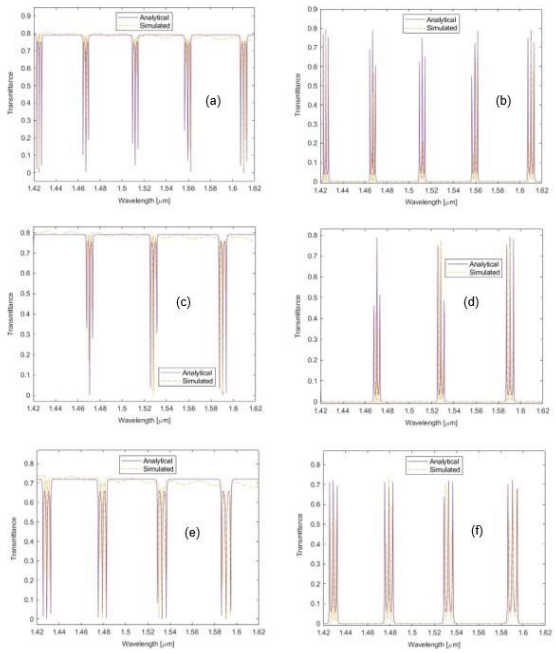

Figure 12 – Transmittances of the TRR models:

(a) – port 2 and (b) – port 3 : with a *r* = 2,5 μm.

(c) – port 2 and (d) – port 3 : with a radius of 2,0 μm.

(e) – port 2 and (f) – port 3 : with a n_{core} of 2,74.

VIII. CONCLUSION

In this research, the description, and the analysis of WDM systems is developed considering 3 main configurations of ring resonators considering the theoretical basis presented in the state-of-the-art and employed in *MATLAB* and the finite element method applied in the *COMSOL Multiphysics* tool.

To do the research on WDM systems, the wave theory is introduced regarding the propagation of light waves, taking into account the characteristics of the medium and the relationship between the fields. These fields are expressed as phasors for plane waves and the theoretical equations are established. Furthermore, the fundamental parameters and sections of planar optical waveguides are also defined. In this waveguides, the conditions for light propagation are presented, namely the equation that specifies the propagation constants of the modes, in which exists transmission of light. A 2D waveguide example, known as slab waveguide, is described, having only two fundamental modes, the transversal electric and transversal magnetic modes. For examining more complex two-dimensional waveguide structures, the finite element method is a more accurate method. Moreover, the effective index method allows the reduction of three-dimensional waveguides onto 2D structures. Besides these methods and for ring resonators, the **coupling** of two or more waveguides are crucial.

The 3 topologies of the ring resonators examined have 2 bus waveguides and an increasing number of ring-shaped waveguides, being one for the first, 2 for the second and three for the last topology. In the state-of-the-art, the theoretical basis of ring resonators and the respective parameters are stated. The signal flow graph along with the Mason's rule is used to obtain the analytical equations for the ratio between the output and input fields, required for the determination of the analytical models of the ring resonators. To compare the output response of the models for the ring resonators with distinct radii and materials, the transmittances of the 2 output ports are determined.

Considering the results of the ring resonators models, the transmittance, except for the resonance peaks, is identical for the 3 topologies with the same dimensions and materials. The main difference between topologies with the same parameters is the number of resonance wavelengths, that is higher due to the increase in the number of ring-shaped waveguides. The decrease in the radii of the ring-shaped waveguides also changes the number of resonance wavelengths for the 3 topologies, with the FSR increase. For models with different core materials, the higher transmittances decrease with lower core refractive indexes and the resonance width increases. Furthermore, the analytical resonance wavelengths are slightly different from the simulated ones. This variation occurs because of the simplifications assumed for the analytical models. The change of the transmittance results, in resonance, between the results from the analytical and simulated models are due to the mean values assumed for the calculus of the coefficients and the approximate solutions obtained.

These results show that the theoretical methods are reliable to do the verification of the output responses for the ring resonators models. Also, the number of waveguides, the core

materials and the radii of ring resonators are parameters which allow the tuning of the output needed for WDM applications. Furthermore, the ring resonators can work as wavelength multiplexers, with the transmission of the resonance wavelengths.

For future research within these WDM analyses for ring resonators, the width of the straight waveguides or the distance between waveguides can be modified.

REFERENCES

[1] O.E. Delange, Wideband optical communication systems, Part II – Frequency division multiplexing, *Proc IEEE*, vol.58, p.1683, October 1970.

[2] Ishio, H., Minowa, J., and K. Nosu, Review and Status of Wavelength-Division-Multiplexing Technology and Its Application, *Journal of Lightwave Technology*, vol. Lt-2, No.4, August 1984.

[3] Keiser, G. E., A Review of WDM Technology and Applications, *Optical Fiber Technology* **5**, 3-39 (1999).

[4] Smit, M. K. and C. Van Dam, "PHASAR-based WDM devices: Principles, design and applications, *IEEE J.Selected Topcis Quantum Electronics*, vol.2, 236, 1996.

[5] Fonjallaz, P.- Y., H. G. Limberger, and R. P. Salanthé, Bragg gratings with efficient and wavelength-selective fiber out-coupling, *J. Lightwave Technol.*, vol.15, 371, 1997.

[6] Okamoto, K., Fundamentals of Optical Waveguides, *Elsevier*, 2021.

[7] Stratton, J. A, Electromagnetic Theory, *New York: McGraw-Hill*, 1941.

[8] Born, M. and E. Wolf, Principles of optics: electromagnetic theory of propagation, interference and diffraction of light, *Elsevier*, 2013.

[9] Marcuse, D., Theory of Dielectric Optical Waveguides, *New York: Academic Press*, 1974.

[10] https://www.intechopen.com/chapters/61838, visited in 2023.

[11] Huang, W. P., Coupled-mode theory for optical waveguides: an overview, *J. Opt. Soc. Am. A*, Vol.11, No.3, March 1994.

[12] Stokes, L. F., M. Chorodow, and H. J. Shaw, All-single-mode fiber resonator, *Opt. Lett*, 7:288-290, 1982.

[13] Heebner, J. E., V. Wong, A. Schweinsberg, R. W. Boyd, and D. J. Jackson, Optical Transmission Characteristics of Fiber Ring Resonators, *IEEE Journal of Quantum Electronics*, vol.40, no.6, June 2004.

[14] Yariv, A., Critical Coupling and Its Control in Optical Waveguide - Ring Resonator Systems, *IEEE Photonics Technology Letters*, vol.14, no.4, April 2002.

[15] Van, V., T. A. Ibrahim, K. Ritter, P. P. Absil, F. G. Johnson, R. Grover, J. Goldhar, and P.- T. Ho, All-optical nonlinear switching in GaAs-Al-GaAs microring resonators, *IEEE Photon. Technol. Lett.*, vol.14, pp.74-77, January 2002.

[16] Heebner, J. E., and R. W. Boyd, Enhanced all-optical switching by use of a nonlinear fiber ring resonator, *Opt. Lett.*, vol.24, pp.847-849, 1999.

[17] Boyd, R. W., and J. E. Heebner, Sensitive disk-resonator photonic biosensor, *Appl. Opt.*, vol.40, pp.5742-5747, 2001.

[18] McCall, S. L., A. F. J. Levi, R. E. Slusher, S. J. Pearton, and R. A. Logan, Whispering-gallery mode microdisk lasers, *Appl. Phys. Lett.*, vol.60, pp. 289-291, 1992.

[19] Little, B. E., S. T. Chu, A. Haus, J. Foresi, and J. -P. Laine, Microring resonator channel dropping filters, *J. Lightwave Technol.*, vol.15, pp.998-1005, April 1997.

[20] Afroozeh A., I. S. Amiri, K. Chaudhary, J. Ali, and P. P. Yupapin, Analysis of Optical Ring Resonator, *Advances in Laser and Optics Research*, vol. 11, ch.6, 2015.

[21] Rabus, D. G., Ring Resonators: Theory and Modeling, *Integrated Ring Resonators*, 2007.

[22] Weber, H., and R. Ulrich, A Thin-Film Ring Laser, *Applied Physics Letters*, pp.38-40, 1971.

[23] Haavisto, J., and G. Pajer, Resonance effects in low-loss ring waveguides, *Optics Letters*, 1982.

[24] Oda, K., N. Takato, and H. Toba, A wide-FSR waveguide double ring resonator for optical FDM transmission systems, *Journal of Lightwave Technology*, 1991.

[25] Rabiei, P., and W.H. Steier, Micro-ring resonators using polymer materials, *IEEE*, 2001.

[26] Rabiei, P. et al., Polymer micro-ring resonators filters and modulators, *Journal of Lightwave Technology*, 2002.

[27] Hryniewicz, J., et al., Microring resonator notch filters, *IEEE*, 2000.

[28] Wu, D., Y. Wu, Y. Wang, J. An and X. Hu, Reconfigurable optical add-drop multiplexer based on thermally tunable micro-ring resonators, *Optics Communications 367*, 44-49, 2016.

[29] Parandin, F. and N. Bagheri, Design of a 2 x 1 multiplexer with a ring resonator based on 2D photonic crystals, *Optics 11*, 2023.

[30] Jile, H., Application of nonlinear ring resonators for realizing all-optical digital multiplexers, *Photonics and Nanostructures – Fundamentals and Applications 45*, 2021.

[31] Jagota, V., A. P. S. Sethi, and K. Kumar, Finite Element Method: An Overview, *Walailak Journal*, 2013.

[32] Clough, R. W., The finite element method in a plane stress analysis, *Proceedings of the 2nd ASCE Conference on Electronic Computation*, 1960.

[33] Courant, R., Variational methods for the solutions of equilibrium and vibrations, *Bull. Am. Math, Soc.*, **49**, 1-23, 1943.

[34] Hrenikoff, A., Solution of problems in elasticity by the framework method, *J. Appl. Mech*, 1941.

[35] Zienkiewicz, C., and Y. K. Cheung, Finite elements in the solution of field problems, *Engineer*, **220**, 507-10, 1965.

[36] https://www.jousefmurad.com/fem/the-finite-element-method-beginners-guide, visited in 2023.

[37] Lameirinhas, R. A. M., J. P. N. Torres, A. Baptista, and M. J. M. Martins, The impact of nanoantennas on ring resonators' performance, *Optics Communications 490*, 2021.

[38] Hiremath, K. R., Coupled mode theory based modeling and analysis of circular optical microresonators, 2005.

[39] https://refractiveindex.info, visited in 2023.

[40] Marple, D. T. F., Refractive index of ZnSe, ZnTe and CdTe, *J. Appl. Phys.* **35**, 539-542, 1964.

[41] Yupapin, P. P., Saeung, P. and Chaichuay, C., The serially coupled multiple ring resonator filters and Vernier effect, *Optica Applicata*, Vol XXXIX, No.1, January 2009.

[42] Mason, S. J., Feedback theory-further properties of signal flow graphs, *Proceedings of the IRE*, **44**(7), 920-926, 1956.